Cell Reports
Article

The H3K27 Demethylase JMJD3 Is Required for Maintenance of the Embryonic Respiratory Neuronal Network, Neonatal Breathing, and Survival

Thomas Burgold,[1] Nicolas Voituron,[3,6,7] Marieta Caganova,[2,6] Prem Prakash Tripathi,[1,6] Clement Menuet,[3] Betsabeh Khoramian Tusi,[1,8] Fabio Spreafico,[1] Michelle Bévengut,[3] Christian Gestreau,[3] Serena Buontempo,[1] Antonio Simeone,[4] Laurens Kruidenier,[5] Gioacchino Natoli,[1] Stefano Casola,[2] Gérard Hilaire,[3] and Giuseppe Testa[1,*]

[1]European Institute of Oncology (IEO)
[2]FIRC Institute of Molecular Oncology Foundation (IFOM)
IFOM-IEO Campus, Via Adamello 16, 20139 Milan, Italy
[3]Mp3-respiration, Centre de Recherche en Neurobiologie et Neurophysiologie de Marseille, Unité Mixte de Recherche 6132 CNRS-Université Aix-Marseille II et III, Faculté Saint Jérôme, 13397 Marseille Cedex 20, France
[4]CEINGE Biotecnologie Avanzate, Via Comunale Margherita 482, 80145 and Institute of Genetics and Biophysics "A. Buzzati-Traverso," National Research Council, Via Pietro Castellino 111, 80131 Naples, Italy
[5]Epinova DPU, Immuno-Inflammation Therapy Area, GlaxoSmithKline R&D, Medicines Research Centre, Gunnels Wood Road, Stevenage SG1 2NY, UK
[6]These authors contributed equally to this work
[7]Present address: Laboratoire Réponses Cellulaires et Fonctionnelles à l'Hypoxie, EA 2363 UFR Santé, Médecine, Biologie Humaine, Université Paris 13, 74 rue Marcel Cachin, 93017 Bobigny Cedex, France
[8]Present address: University of Florida College of Medicine, Gainesville, FL 32611, USA
*Correspondence: giuseppe.testa@ieo.eu
http://dx.doi.org/10.1016/j.celrep.2012.09.013

SUMMARY

JMJD3 (KDM6B) antagonizes Polycomb silencing by demethylating lysine 27 on histone H3. The interplay of methyltransferases and demethylases at this residue is thought to underlie critical cell fate transitions, and the dynamics of H3K27me3 during neurogenesis posited for JMJD3 a critical role in the acquisition of neural fate. Despite evidence of its involvement in early neural commitment, however, its role in the emergence and maturation of the mammalian CNS remains unknown. Here, we inactivated *Jmjd3* in the mouse and found that its loss causes perinatal lethality with the complete and selective disruption of the pre-Bötzinger complex (PBC), the pacemaker of the respiratory rhythm generator. Through genetic and electrophysiological approaches, we show that the enzymatic activity of JMJD3 is selectively required for the maintenance of the PBC and controls critical regulators of PBC activity, uncovering an unanticipated role of this enzyme in the late structuring and function of neuronal networks.

INTRODUCTION

Posttranslational modifications of histone tails have been associated, and at times causally linked, to transcriptional outcomes. Due to its comparative stability over other modifications (Byvoet et al., 1972), lysine methylation was initially proposed as an ideal candidate to mediate the epigenetic maintenance of transcriptional states in both replicating and postmitotic cells. In particular, di- and trimethylation of lysine 27 on histone H3 (H3K27me2/3) by EZH2 within Polycomb repressive complex 2 (PRC2) has emerged as a critical mechanism of gene repression and, more recently, as a bona fide epigenetic mark that can be propagated through cell division (Hansen et al., 2008; Margueron et al., 2009). Two lines of experimentation revealed, however, the unexpected dynamics of this mark: (1) the identification of H3K27me2/3-specific JmjC-domain demethylases JMJD3 and UTX (Agger et al., 2007; Burgold et al., 2008; De Santa et al., 2007; Jepsen et al., 2007; Lan et al., 2007; Xiang et al., 2007); and (2) the description of genome-wide changes in H3K27me3 that accompany the entire process of neural fate acquisition (Mohn et al., 2008). The developing CNS has indeed become a paradigm-setting model to interrogate how H3K27me3-mediated repression times the activity of critical regulators of neurogenesis, as shown through the ablation of *Ezh2* at different stages of corticogenesis whose divergent phenotypes of delayed or accelerated neurogenesis (Hirabayashi et al., 2009; Pereira et al., 2010) were recently reconciled in a model of Polycomb-mediated developmental timing that reflects both the epigenetic transmission of the mark and its dynamic relocation to new targets (Testa, 2011). Conversely, the exquisite sensitivity of neurogenesis to modulation of H3K27me3 underscores the relevance of timed H3K27me3 demethylation, as revealed by the critical role of JMJD3 in both mouse embryonic stem cell (ESC) neurulation (Burgold et al., 2008) and chick spinal cord neurogenesis (Akizu et al., 2010). Yet, despite these early advances the relevance of JMJD3 for the function of the mammalian CNS in vivo remains to be explored and nothing is known about its role in later stages of CNS development and in neuronal maturation.

Here, we inactivated *Jmjd3* in the mouse to study its function in CNS emergence and maturation, and we describe a specific function of its enzymatic activity in the maintenance of the respiratory rhythm generator (RRG).

The perinatal RRG is hypothesized to be formed by two coupled oscillators, the retrotrapezoid nucleus/parafacial respiratory group (RTN/pFRG) and the pre-Bötzinger complex (PBC). The PBC, ventral to the nucleus ambiguus (nA), functions from embryonic day 15.5 (E15.5) and possibly constitutes the primary respiratory oscillator (Fortin and Thoby-Brisson, 2009; Onimaru et al., 2009; Smith et al., 1991; Thoby-Brisson et al., 2009). The RTN/pFRG, ventral to the facial motor nucleus (nVII), functions as early as E14.5, is CO_2/pH chemosensitive and may be a secondary oscillator (Thoby-Brisson et al., 2009).

Genetic manipulation led to the identification of several genes that contribute to RRG emergence and function. *MafB* or *Math1* inactivation drastically alters the PBC rhythm without abolishing it (Blanchi et al., 2003; Rose et al., 2009). Inactivation of *Phox2b*, *Tshz3*, or *Task2* affects instead RTN/pFRG chemosensibility, again disturbing but not abolishing PBC rhythm (Amiel et al., 2009; Caubit et al., 2010; Gestreau et al., 2010). Inactivation of *Maoa*, *Phox2a*, and *Necdin* affects the monoaminergic system, which disturbs RRG maturation but does not silence the PBC (Bou-Flores et al., 2000; Viemari et al., 2004; Zanella et al., 2008). Finally, only two mutants were identified thus far with totally silenced RRG, the *VGlut2* mutant and the *Dbx1* mutant, where PBC neurons fail to achieve synchronous activation and to elaborate central respiratory drive (Bouvier et al., 2010; Wallén-Mackenzie et al., 2006). Here, we show that JMJD3 enzymatic activity is critical for RRG maintenance and that JMJD3 controls the expression of specific markers and critical regulators of PBC function. Lack of JMJD3 did not impair the early emergence of the RRG at E15.5, but specifically altered the maintenance of its PBC component, totally silencing it at E18.5 and leading to neonatal death with full penetrance.

RESULTS

Loss of JMJD3 Results in Perinatal Lethality

We inactivated *Jmjd3* in the mouse starting from a gene trap ESC line in which the first noncoding exon of the *Jmjd3* transcript had been trapped by a splice-acceptor (sA)-based knockout cassette. We mapped its integration to intron 1 (Figure 1A) and devised a PCR-based strategy to discriminate the heterozygous from the homozygous state of the *Jmjd3* knockout allele in the mice that we derived through blastocyst injection (Figure 1B). In heterozygous crosses, we recovered no homozygous knockout animals at weaning age (Figure 1C). We thus went back to earlier developmental stages and retrieved homozygous knockout fetuses up to embryonic day E18.5, indicating that loss of JMJD3 results in perinatal or neonatal lethality. In the light of JMJD3 function in early development, this surprising finding prompted us to evaluate the impact of the gene trap cassette on JMJD3 expression at the onset of development. We derived ESC lines from heterozygous crosses and found that *Jmjd3*$^{-/-}$ ESC still expressed nearly half the amount of JMJD3 as their wild-type controls, suggesting that in ESC (Figure 1D) the trap cassette had been partially circumvented through alternative promoters. RT-PCR confirmed that while transcripts spanning the exon1-exon2 junction were absent in *Jmjd3*$^{-/-}$ ESC, the downstream exon combinations were still present (Figure 1E), though *Jmjd3* transcript levels were reduced by 4- to 5-fold and decreased further to less than 10-fold during CNS development (Figure 1F). We confirmed the virtually complete ablation of *Jmjd3* expression during development also by RNA in situ hybridization with a probe located at the 3′ end of the gene. As shown in Figure 1G, at embryonic day E16.5 *Jmjd3* is broadly expressed, with particularly high levels in various sites of the CNS, including the cortex, the basal ganglia, the olfactory epithelium, and the cerebellar primordium. In mutant embryos, *Jmjd3* expression was instead almost completely ablated, indicating that the most upstream promoter of *Jmjd3* is the dominant one in most tissues.

Jmjd3-Null Mice Die at Birth of Respiratory Failure

In order to determine the cause of perinatal lethality in *Jmjd3*-null pups, we followed the natural delivery of several litters (n = 14) taking care not to disturb maternal care. *Jmjd3*-null neonates had normal weight and morphology but most of them did not breathe, quickly became cyanotic, and died right after birth or were found already dead (Figures 2A and 2B). A few survived for several hours (n = 8/32, $\leq$12 hr) and only a tiny minority survived longer than 12 hr but less than 1 day (n = 3/32, $\leq$ 24 hr) (Figure 2A). In these few pups, the tissue architecture of the lungs was unaffected, with normally inflated alveolar spaces, thus excluding a primary lung defect as the cause of respiratory failure (Figure S1). Exteriorization at E18.5 revealed that most wild-type and heterozygous embryos breathed and survived, whereas all *Jmjd3*-null embryos rapidly died, without producing any discernible respiratory efforts. We further examined breathing behavior in four litters from heterozygous crosses using whole-body plethysmography (Figures 2C–2E). Following exteriorization at E18.5, *Jmjd3*$^{+/+}$ and *Jmjd3*$^{+/-}$ embryos (n = 12/22 in total) first gasped for 2–5 min, producing deep respiratory movements involving the whole-body muscles at a slow frequency (about 2–5 cycles per minute [c.min]$^{-1}$), and thereafter displayed normal, shallow breathing at a faster frequency (46 ± 7 c.min^{-1}; Figure 2E). Plethysmography never revealed any gasps or normal respiratory movements in *Jmjd3*$^{-/-}$ embryos (n = 8/8; Figure 2E). To exclude heart failure as the primary cause for death in *Jmjd3*$^{-/-}$ mice, we recorded the electrocardiogram (ECG) of E18.5 embryos kept in utero (Figure S2). The heart was regularly beating in *Jmjd3*$^{-/-}$ (n = 5) and *Jmjd3*$^{+/+}$ or *Jmjd3*$^{+/-}$ (n = 10) embryos (102 ± 17 c.min^{-1} and 68 ± 9 c.min^{-1}, respectively). To exclude muscular or neuromuscular dysfunctions as causes for the lack of breathing in *Jmjd3*-null embryos, single electrical shocks were applied to the diaphragm or the phrenic nerve of embryos and induced chest movements (data not shown).

The Respiratory Rhythm Generator Does Not Function in *Jmjd3*-Null Embryos at E18.5

Given the proficiency of the cardiac and the peripheral respiratory systems in *Jmjd3*-null embryos, we suspected a deficit in the RRG and used en bloc medullary preparations of exteriorized embryos at E18.5 to examine whether the isolated RRG of

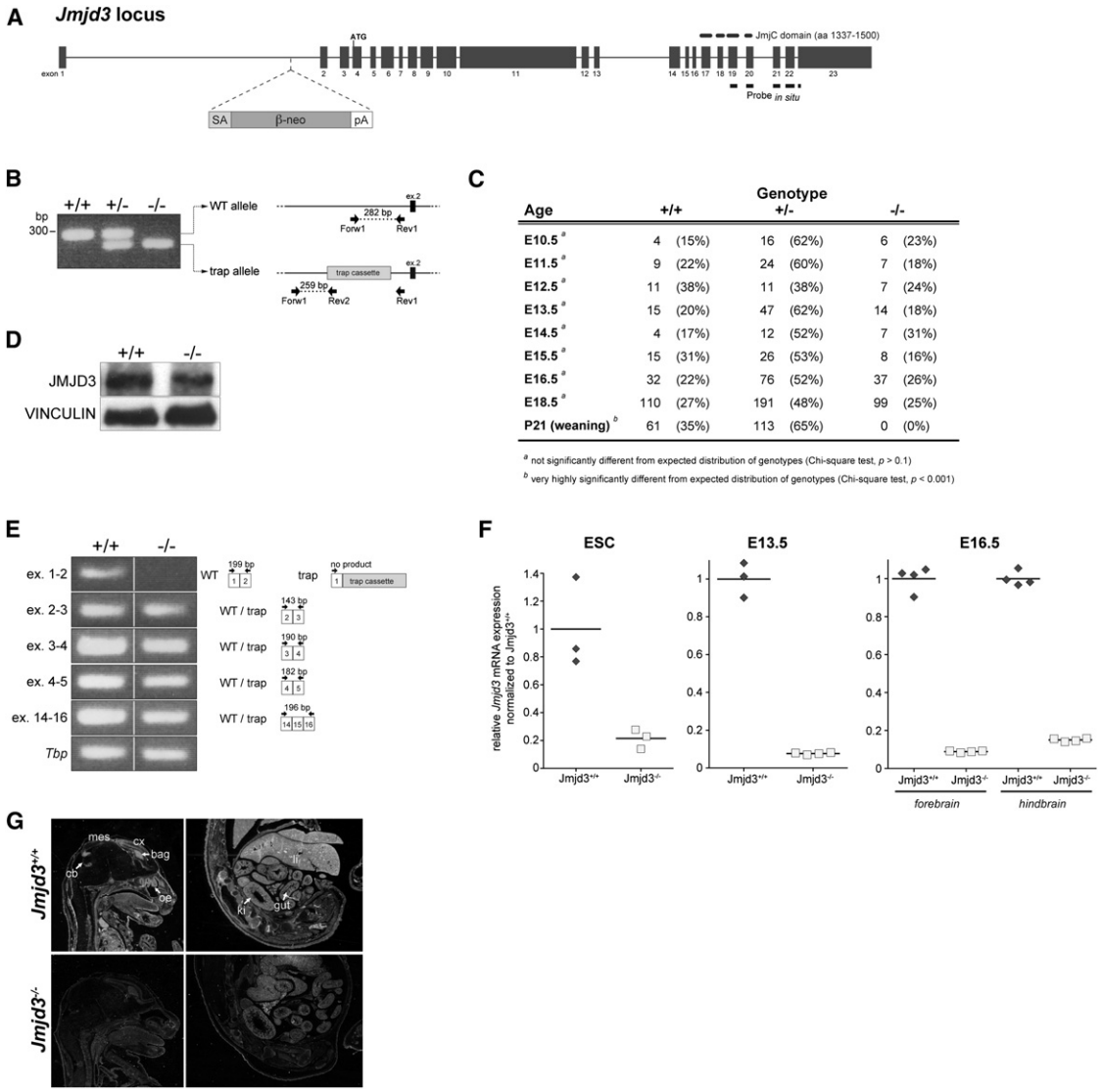

Figure 1. Inactivation of *Jmjd3*

(A) Scheme of the mouse *Jmjd3* locus showing exons along with the integration site of the trap cassette, which comprises a splice acceptor (SA), the β-galactosidase neomycin resistance gene fusion (β-geo) and a polyadenylation signal (pA). The probe used to assess *Jmjd3* expression by RNA in situ hybridization ($Probe_{in\ situ}$) is indicated by black bars below 3′ terminal exons. The JmjC domain is shown mapped onto the relevant exons (17–20).

(B) Triplex PCR-based genotyping of wild-type (+/+), heterozygous (+/−), and homozygous (−/−) littermates (left). The scheme on the right shows the position of the three primers, with the Forw1/Rev1 product amplified from the wild-type allele (282 bp), and the Forw1/Rev2 product amplified from the trapped allele (259 bp).

(C) Table showing the number of wild-type, heterozygous and homozygous embryos at the indicated stage of development (E10.5–E18.5) and of pups at weaning age (P21). Statistical analysis was performed with Chi-square test.

(D) Western blot analysis of JMJD3 expression in wild-type and homozygous mutant ESC clones. Vinculin served as loading control.

(E) Identification of *Jmjd3* transcript variants by RT-PCR. In $Jmjd3^{-/-}$ ESC, no product was detected for the primer pair spanning exons 1 and 2. All other primer combinations yielded a product in *Jmjd3* mutant ESCs. *Tbp* served as housekeeping control.

(F) qRT-PCR analysis of *Jmjd3* mRNA expression in ESCs, E13.5 brains and E16.5 forebrains and hindbrains. *Tbp* served as housekeeping control.

(G) RNA in situ hybridization showing *Jmjd3* expression on sagittal sections of $Jmjd3^{+/+}$ and $Jmjd3^{-/-}$ embryos at E16.5 of embryogenesis. $Jmjd3^{+/+}$ embryos (upper row) showed *Jmjd3* expression in the cortex (cx), cerebellum (cb), mesencephalon (mes), basal ganglia (bag), and the olfactory epithelium (oe) as well as in liver (li), gut (gut), and kidney (ki). In $Jmjd3^{-/-}$ mutants (lower row) the signal was absent or barely detectable, indicating virtually complete loss of the *Jmjd3* transcript.

Jmjd3-null embryos was able to produce respiratory-like phrenic bursts (PBs) in vitro (Blanchi et al., 2003; Caubit et al., 2010) (Figure 3A). Rhythmic PBs were commonly recorded in all $Jmjd3^{+/+}$ (n = 6/6) and most $Jmjd3^{+/-}$ (n = 14/18) preparations (12 ± 4 $c.min^{-1}$ and 10 ± 1 $c.min^{-1}$, respectively) but never in $Jmjd3^{-/-}$ preparations (n = 8/8; Figures 3B and 3C).

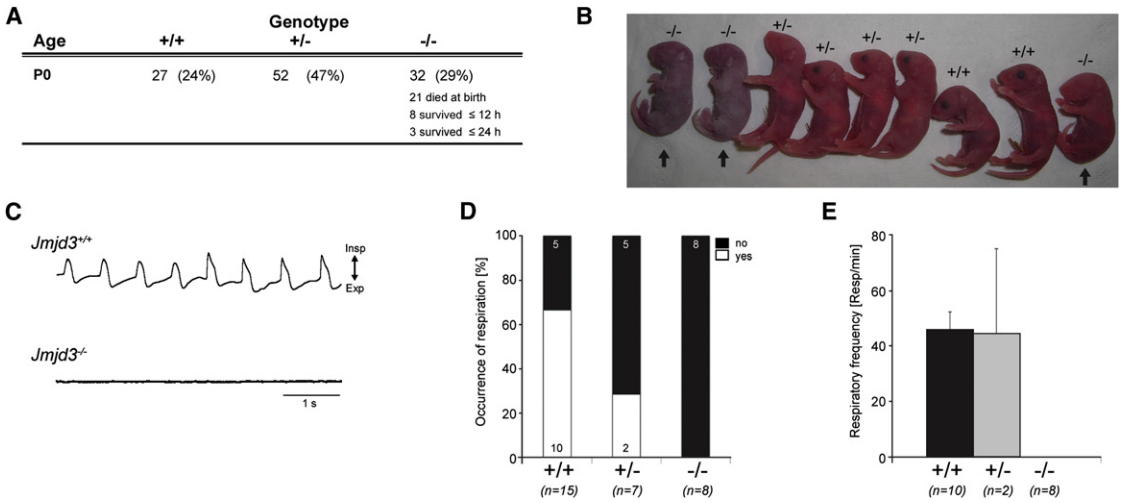

Figure 2. Perinatal Lethality and Respiratory Failure upon Loss of JMJD3

(A) Table showing the number of *Jmjd3*$^{+/+}$, *Jmjd3*$^{+/-}$, and *Jmjd3*$^{-/-}$ neonates at birth (P0). Out of 32 *Jmjd3*$^{-/-}$ neonates, most (21) were born dead or died at birth, few mice (eight) died within the first 12 hr postpartum and only three survived longer than 12 hr but less than 24 hr.

(B) Picture showing the appearance of neonates from heterozygous crosses immediately after birth. The two cyanotic neonates (first two in the row) were born dead and afterward confirmed as *Jmjd3*$^{-/-}$, a third *Jmjd3*$^{-/-}$ neonate survived for 20 hr (last pup in the row).

(C) Plethysmographic recordings of breathing activity in vivo from surgically delivered *Jmjd3*$^{+/+}$ and *Jmjd3*$^{-/-}$ E18.5 fetuses. All wild-type mice initiated respiratory cycles of inspirations (upward deflections) and expirations (downward deflections), whereas none of the *Jmjd3*$^{-/-}$ littermates showed any sign of ventilation.

(D) Histogram showing for wild-type, heterozygous and mutant genotypes the percentage of surgically delivered E18.5 embryos that did (white bar) or did not (black bar) show respiratory activity. The number of mice analyzed is indicated in each bar.

(E) Quantification of respiratory frequency indicated in respirations per minute. Bars represent the mean ± SEM of the numbers (n) of mice indicated on the x axis below the graph.

See also Figure S1.

The lack of rhythmic PBs in *Jmjd3*$^{-/-}$ preparations could result from either an inactive RRG or a failure in synaptic transmission from the RRG to the spinal phrenic motor neurons. To distinguish between these possibilities, we electrically stimulated either the spinal cord or the medulla in *Jmjd3*$^{-/-}$ preparations. As depicted in Figure 3D, we applied single electrical shocks at the level of the second cervical segment of the spinal cord to activate the respiratory output pathways running from the medullary respiratory areas toward the phrenic motor neurons (St2) and recorded the activation of phrenic motor neurons at the level of the fourth cervical segment (C4). This stimulation induced a short latency response of phrenic motor neurons in both *Jmjd3*$^{-/-}$ and *Jmjd3*$^{+/+}$ preparations, revealing that *Jmjd3*$^{-/-}$ phrenic motor neurons responded to spinal synaptic excitation (Figure 3G). Second, we applied electrical shocks to the medulla (St1 in Figure 3D), close to respiratory related areas (150–200 μm below the surface of the ventrolateral medulla). In wild-type preparations, as previously reported (Blanchi et al., 2003), medullary stimulation induced brief responses of phrenic motor neurons and, when delivered during the second third of expiration, it shortened the silent expiratory period and precipitated the onset of the next PB (Figure 3D, upper trace). Instead in *Jmjd3*$^{-/-}$ preparations, the medullary stimulation never induced a PB (Figure 3D, lower trace) but commonly induced brief responses of phrenic motor neurons (Figure 3E). The phrenic responses to spinal and medullary stimulations were observed from both ipsilateral and controlateral sides, revealing normally crossed pathways in *Jmjd3*$^{-/-}$ preparations. When applying long train of shocks (3 s at 100 Hz) to either the ventrolateral medulla or the median raphe area, we observed sustained and long-lasting discharges of phrenic roots, persisting over several seconds (Figure 3F), but never rhythmic PB.

Thus, given the ability of *Jmjd3*$^{-/-}$ phrenic motor neurons to respond to synaptic inputs from spinal and medullary regions and even to fire for long periods, the lack of rhythmic PB was indicative of a defective or quiescent RRG. We attempted to activate the RRG of *Jmjd3*$^{-/-}$ preparations by applying acidified artificial cerebrospinal fluid (aCSF) (n = 2) or aCSF containing either serotonin (25 μM; n = 2) or norepinephrine (25 μM; n = 2) or elevated concentration of potassium (9 mM; n = 2) to the medulla. None of these experimental maneuvers induced rhythmic PB (data not shown), arguing for a defective rather than quiescent RRG.

Disruption of the Pre-Bötzinger Complex in E18.5 *Jmjd3*-Null Embryos

We next investigated whether the functional deficit in the RRG could be traced to a neuroanatomical defect in *Jmjd3*$^{-/-}$ embryos. For this, we conducted an immunohistochemical analysis of the neurons organized in the two hypothesized coupled oscillators of the murine RRG, the PHOX2b-positive neurons of the RTN/pFRG and the Neurokinin 1 receptor

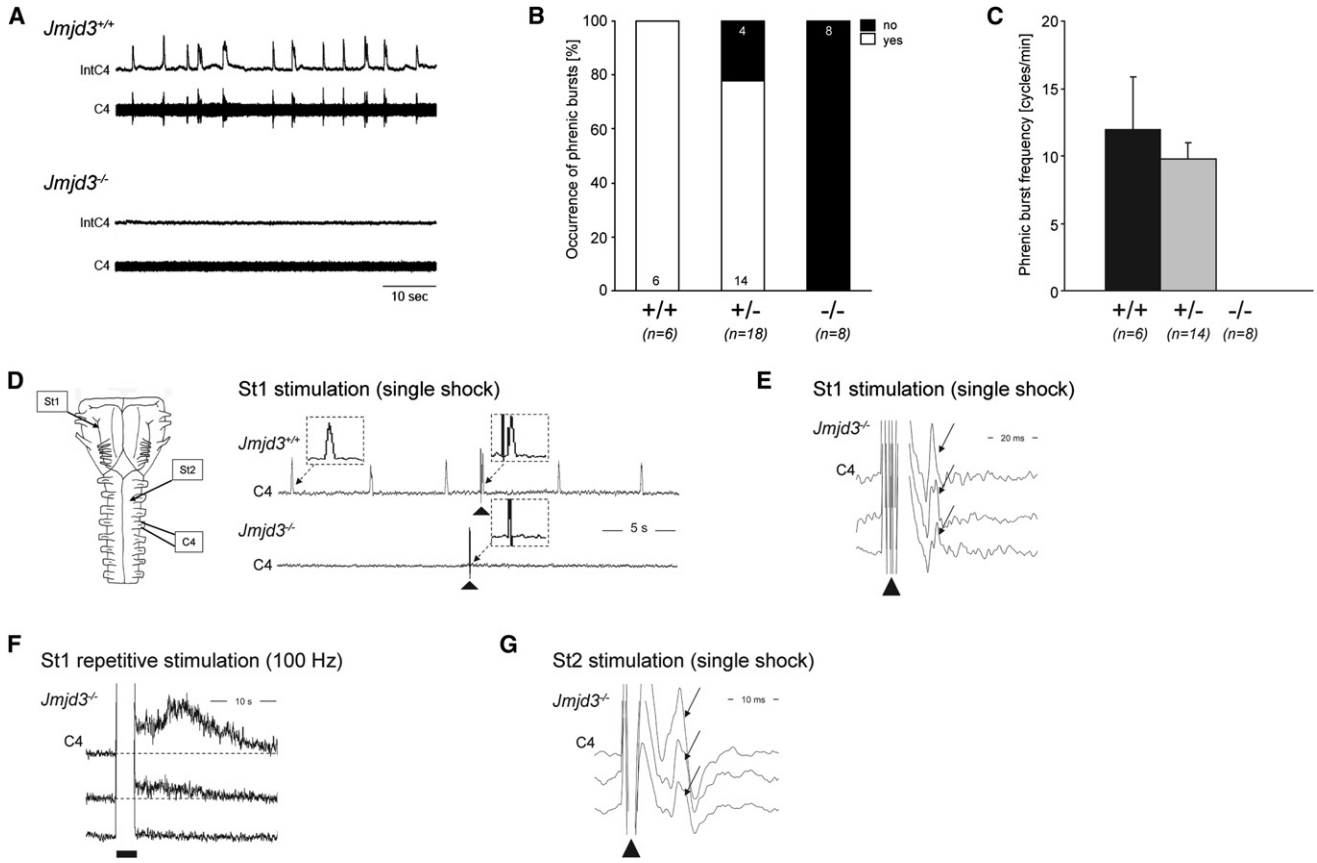

Figure 3. Lack of Respiratory Bursts in *Jmjd3*$^{-/-}$ Medullary In Vitro Preparations

Medullary in vitro (*en bloc)* preparations from *Jmjd3*$^{-/-}$ embryos surgically delivered at E18.5 do not produce rhythmic phrenic bursts although phrenic motor neurons are synaptically excitable by electrical stimulations of the medulla and spinal cord.

(A) Paired traces show raw (C4) and integrated (IntC4) signals recorded from the phrenic nerve of medullary in vitro preparations isolated from *Jmjd3*$^{+/+}$ and *Jmjd3*$^{-/-}$ embryos (upper and lower traces, respectively) surgically delivered at E18.5.

(B) Histogram showing the percentage of *Jmjd3*$^{+/+}$, *Jmjd3*$^{+/-}$, and *Jmjd3*$^{-/-}$ E18.5 brainstem preparations that did (white bars) or did not (black bars) produce rhythmic phrenic bursts (the number of preparations analyzed is indicated in each bar).

(C) Quantification of phrenic burst frequency expressed in cycles per minute. Bars represent the mean ± SEM of the numbers (n) of mice indicated on the x axis below the graph.

(D) Schematic drawing of the en bloc embryonic preparation (ventral surface upward) showing the medullary (St1) and spinal (St2) stimulation sites and the phrenic nerve recording site at the level of the C4 ventral root (C4). Upper and lower traces show the presence and absence of rhythmic phrenic bursts (integrated C4 signal) in preparations of *Jmjd3*$^{+/+}$ and *Jmjd3*$^{-}$ E18.5 embryos, respectively. Applying a single shock electrical stimulation (1 ms, 2 V; black triangle) at the medullary St1 site during expiration (silent phrenic interval) triggered a premature phrenic burst in *Jmjd3*$^{+/+}$ but not in *Jmjd3*$^{-/-}$ preparations. Inserts (enlarged time scale: 1 s) show spontaneous and stimulation-induced phrenic bursts in the *Jmjd3*$^{+/+}$ preparation and the lack of phrenic burst after stimulation in the *Jmjd3*$^{-/-}$ preparation.

(E) In E18.5 *Jmjd3*$^{-/-}$ preparations, superimposed traces (raw C4 signal) show that single shock stimulations delivered in the medulla at St1 (1 ms, 2 V; black triangle) induced brief synaptic responses of phrenic motor neurons (arrows).

(F) In E18.5 *Jmjd3*$^{-/-}$ preparations, applying repetitive stimulation (100 Hz for 3 s; black bar) to St1 induced long-lasting discharges (integrated C4 signal) of the previously silent phrenic motor neurons, but no rhythmic phrenic bursts. The amplitude and the duration of the stimulation-induced discharges depended on the stimulus strength (from top to bottom, 3, 1.5 and 1 V; pulse duration 1 ms). Dotted lines indicate baseline level of the C4 signal prior to stimulation.

(G) as in (E), but following stimulation of the spinal cord at the level of St2 (1 ms, 2 V; black triangle). In E18.5 *Jmjd3*$^{-/-}$ preparations, superimposed traces (raw C4 signal) show that single shock stimulations at St2 induced short-lasting responses of phrenic motor neurons (arrows).

See also Figure S2.

(NK1R)/Somatostatin (SST)-positive neurons of the PBC. The embryonic PBC has been previously defined through NK1R and SST expression below the nA, extending toward the ventral surface of the medulla at the level of the inferior olive (Blanchi et al., 2003; Caubit et al., 2010; Gray et al., 2001, 2010; Stornetta et al., 2003). We confirmed this PBC-typical distribution in wild-type embryos but not in *Jmjd3*$^{-/-}$ embryos where the corresponding area appeared grossly altered in extension and structure. As shown in Figure 4A, NK1R-positive (left column) and SST-positive (middle column) neurons were present ventrally of the nA of *Jmjd3*$^{-/-}$ medulla, but they were significantly fewer than in the wild-type counterpart, with a much weaker density

and a diffuse, unstructured distribution of the NK1R and SST signals. This was particularly prominent for the subset of NK1R/SST coexpressing neurons, which was recently defined as the core of the PBC in mice (Gray et al., 2010). Complete acquisition of coronal sections enabled the three-dimensional reconstruction and volumetric measurement of the NK1R-positive network of neurons comprising the nA and the PBC (Figure 4B; Movie S1), confirming the stark alterations in the volume and shape of the PBC in *Jmjd3*$^{-/-}$ samples. These abnormalities were reflected also in the distribution of PBC neurons coexpressing SST with PAX2, one of three transcription factors (along with PHOX2b and LHX9) expressed in the ventrolateral medulla (VLM) in specific neuronal subsets (Gray et al., 2004, 2010). As shown in Figure 4C, the number of SST/PAX2 coexpressing neurons was severely reduced in *Jmjd3*$^{-/-}$ PBCs, as determined by serial sectioning and counting along the rostrocaudal axis of the medulla. Given that, in the same regions of *Jmjd3*$^{-/-}$ ventrolateral medulla, the overall number of PAX2-positive neurons was only marginally affected (with a significant reduction only in the uppermost caudal PBC, Figure 4D), the selective alteration in SST/PAX2-double-positive neurons points to a specific requirement for JMJD3 in this specific neuronal subpopulation. Consistently, we also did not observe any significant decrease in the overall number of glutamatergic neurons, as identified through VGLUT2 expression (Figure S3A). Finally, global levels of H3K27me3 were not affected in mutant PBC neurons, as expected on the basis of convergent evidence from several cell types in which JMJD3 was shown to control locus-specific rather than global H3K27me3 (De Santa et al., 2009) (Figure S3B).

In the light of the neuroanatomical alterations of the PBC, we asked whether loss of JMJD3 affected also the RTN/pFRG. As shown in Figure S3C, we identified the expected group of PHOX2b-expressing neurons in the RTN/pFRG area, ventrally of the VII motor nucleus, in both *Jmjd3*$^{+/+}$ and *Jmjd3*$^{-/-}$ embryos, and no differences were observed in PHOX2b and NK1R expression and in the overall structure of the RTN/pFRG (Figure S3C). Consistently, we found the expression of *Jmjd3* in the brainstem to be predominant in the PBC, nA, and nVII and comparatively much lower if barely detectable in the RTN/pFRG (Figures 4E and S3D). Thus, the differential involvement of the two medullary oscillators in our mutants points to a specific requirement for JMJD3 in PBC integrity at E18.5, consistent with its predominant expression pattern.

JMJD3 Is Required for the Maintenance of the Pre-Bötzinger Complex

The embryonic RRG emerges functionally at embryonic days E15.5 and E14.5, respectively, for the coupled PBC and RTN/pFRG respiratory oscillators (Thoby-Brisson et al., 2005, 2009). Because our immunohistochemical analysis showed an altered PBC in the presence of a normal RTN/pFRG at day E18.5, we conducted electrophysiological experiments at earlier embryonic stages to probe the role of JMJD3 in the functional emergence of both oscillators.

At E16.5, a total of 70 embryos from six litters were analyzed using in vitro medullary preparations retaining the rib cage to allow visualization of respiratory movements and recording of chest electromyogram (EMG) discharges (Ren et al., 2003). Rhythmic chest movements were observed in most wild-type and *Jmjd3*$^{+/-}$ preparations (n = 14/16 and 32/34, respectively) as well as in half of the *Jmjd3*$^{-/-}$ preparations (n = 10/20; Figure 4F, middle graph), demonstrating that the embryonic RRG can function at this early embryonic age despite the lack of JMJD3. We then extended our study to day E15.5, when most preparations produced rhythmic chest movements, independent of genotype (n = 6/7, 12/13 and 3/4 for *Jmjd3*$^{+/+}$, *Jmjd3*$^{+/-}$, and *Jmjd3*$^{-/-}$ preparations, respectively; Figure 4F, left graph). Together, these results show that whereas with embryonic maturation the ratio of active/inactive preparations remained constant in *Jmjd3*$^{+/+}$ and *Jmjd3*$^{+/-}$ embryos (about 80%, n = 7/8 and 14/18, respectively), it significantly decreased in *Jmjd3*$^{-/-}$ embryos, dropping from 75% at E15.5 to 50% at E16.5 to 0% at E18.5 (Figure 4F, right graph). Figure S3E shows representative EMG recordings of *Jmjd3*$^{+/+}$ and *Jmjd3*$^{-/-}$ preparations at day E15.5, and the complete lack of activity in day E18.5 *Jmjd3*$^{-/-}$ preparations. In order to further dissect the role of JMJD3 in the emergence of the RRG, we then probed the functional features of the chemosensing neurons that were reported to reside in the maturing RTN/pFRG and to be responsive to pH changes from as early as day E15.5–E16.5 (Caubit et al., 2010). We applied acidified aCSF to the medulla of four *Jmjd3*$^{+/+}$ and two *Jmd3*$^{-/-}$ preparations and observed that acidosis increased the frequency of respiratory EMG discharges in half the samples of either genotype (n = 2/4 and n = 1/2 for *Jmjd3*$^{+/+}$ and *Jmd3*$^{-/-}$ preparations, respectively; data not shown).

Finally, we examined the neuroanatomical correlate of the apparently normal functional emergence of the RRG, analyzing the structure of the PBC in *Jmjd3*$^{-/-}$ embryos at day E16.5. Staining for NK1R revealed a comparatively better preservation of the emerging PBC structure in homozygous null embryos with respect to the striking defects observed at day E18.5, consistent with the largely normal function of the emerging PBC in the absence of JMJD3 (Figure 4G). Interestingly, the SST pattern was more severely affected already at E16.5, suggesting either an earlier sensitivity of the NK1R/SST-double-positive neuronal subset to the loss of JMJD3, or a differential impact of JMJD3 on the expression of the two genes. Finally, we did not find evidence of caspase-dependent apoptosis in mutant PBC (data not shown), in agreement with the broadly conserved number of PAX2-positive neurons recovered at E18.5. Together with the distribution of VGLUT2-positive neurons, this confirms that loss of JMJD3 did not cause widespread neuronal loss in the ventral medulla but impacted selectively on the integrity of the NK1R/SST neuronal core within the PBC.

The emergence, function, and maturation of the PBC starting from day E15.5 has been associated with the input of serotonin (5-HT)-specific neurons from the developing midline raphe system, consistent with the well-established role of early 5-HT signal in networks maturation (Gaspar et al., 2003), including RRG maturation (Bou-Flores et al., 2000; Hilaire et al., 2010) and initiation of rhythmic activity in the developing hindbrain (Hunt et al., 2005). We thus investigated the levels of tryptophan, serotonin and its catabolyte, 5-hydroxyindolacetic acid (5-HIAA), in the brainstem of E16.5 *Jmjd3* mutant and control embryos and found a significant decrease of both 5-HT and 5-HIAA upon

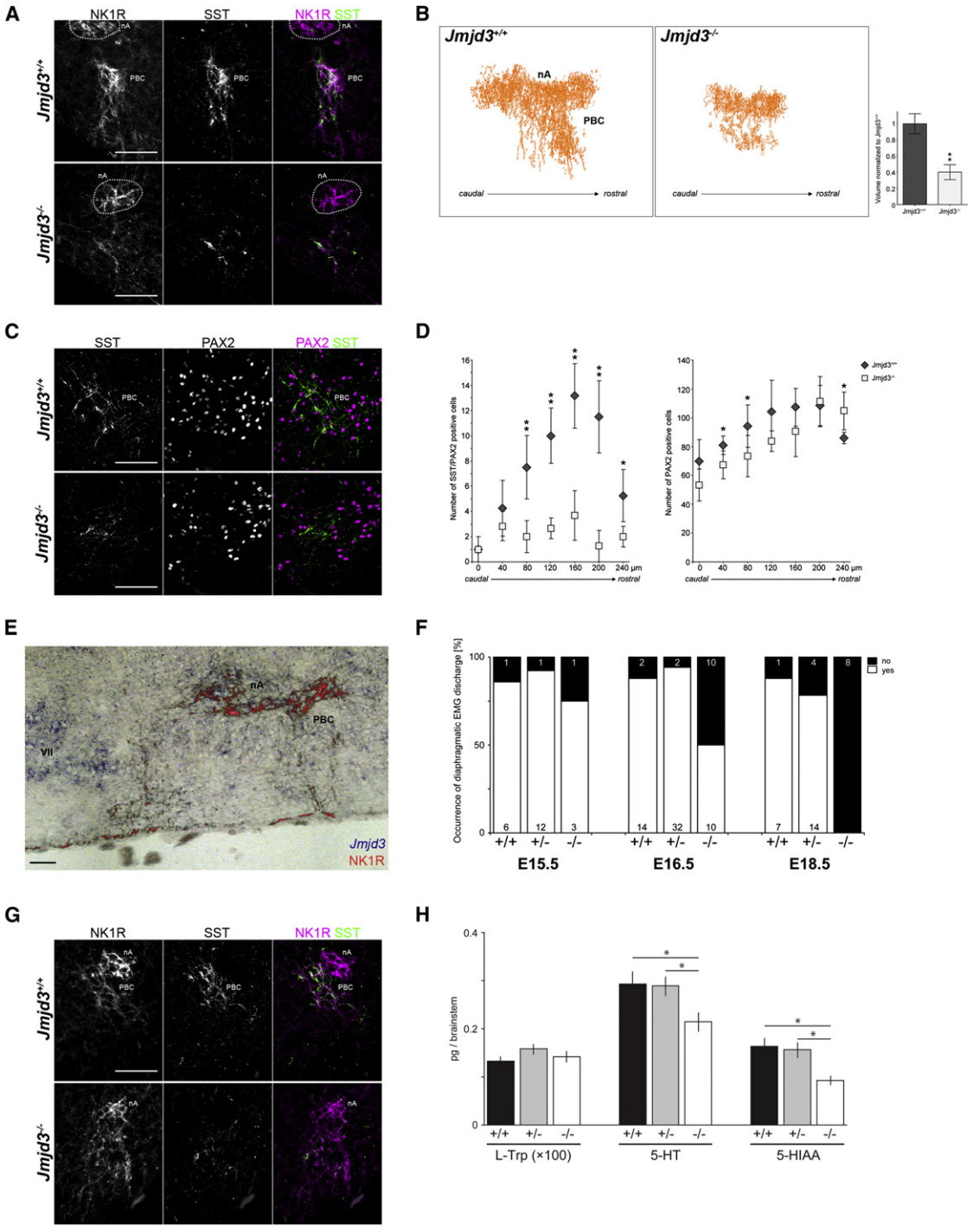

Figure 4. Neuroanatomical Characterization of the Pre-Bötzinger Complex in *Jmjd3*$^{-/-}$ Embryos

(A) Immunohistochemical staining for NK1R (first column) and SST (second column) on coronal sections from wild-type (upper row) and *Jmjd3*$^{-/-}$ (lower row) E18.5 brainstems. A merged image of NK1R (magenta) and SST (green) stainings is shown in the last column on the right.

(B) Three-dimensional reconstruction (in sagittal view, left panels) of the NK1R-positive area comprising the nA and the PBC on consecutive coronal sections of *Jmjd3*$^{+/+}$ and *Jmjd3*$^{-/-}$ E18.5 brainstems. Volumetric measurement, showing the mean ± SD from five wild-type and four mutant E18.5 samples, is shown in the right panel (**$p < 0.01$, Student's t test).

(C) Immunohistochemical staining for SST (first column) and PAX2 (second column) on coronal sections from wild-type (upper row) and *Jmjd3*$^{-/-}$ (lower row) E18.5 brainstems. A merged image of PAX2 (magenta) and SST (green) is shown in the last column on the right.

(D) Graphs showing the number of SST- (left graph) and PAX2- (right graph) positive cells per coronal hemisection at various levels (along the rostrocaudal axis, x axis) of the rostral ventrolateral *Jmjd3*$^{+/+}$ and *Jmjd3*$^{-/-}$ E18.5 medulla. Cells were counted within an area of 260 × 290 μm encompassing the PBC core region

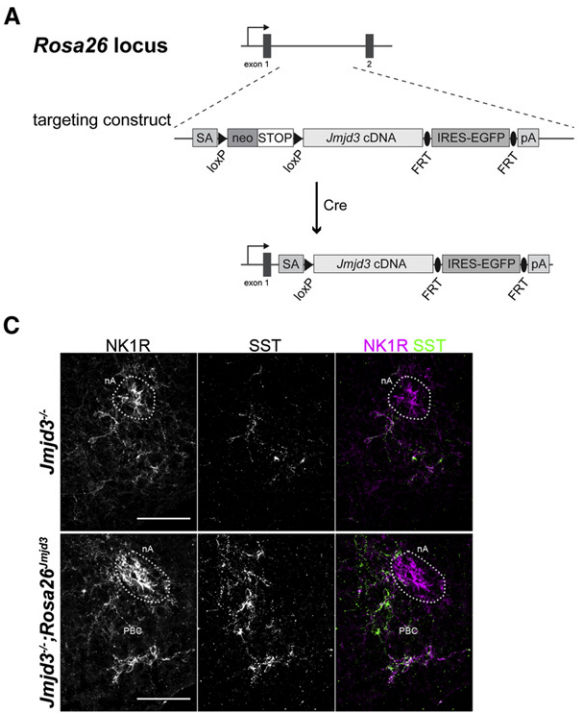

B

Genotype		P21 (weaning)
$Jmjd3^{+/-}$;$Rosa26^{flSTOP\text{-}Jmjd3}$	$Jmjd3^{+/+}$;$Rosa26^{Jmjd3}$	5
×	$Jmjd3^{+/-}$;$Rosa26^{Jmjd3}$	5
$Jmjd3^{+/-}$;Cre	$Jmjd3^{-/-}$;$Rosa26^{Jmjd3}$	13

Figure 5. Exogenous Expression of *Jmjd3* Rescues the Perinatal Lethality of $Jmjd3^{-/-}$ Mutants

(A) Schematic illustration of the targeting strategy to insert the *Jmjd3* transgene into the *Rosa26* locus. The targeting vector contains a splice acceptor site (SA), a loxP-flanked STOP cassette, the *Jmjd3* coding sequence followed by an FRT-flanked IRES-EGFP cassette and a polyadenylation sequence (pA), resulting in Cre-mediated expression of *Jmjd3* from the endogenous *Rosa26* promoter.

(B) Table showing the number of $Jmjd3^{+/+}$, $Jmjd3^{+/-}$, and $Jmjd3^{-/-}$ mice carrying the $Rosa26^{Jmjd3}$ allele that were recovered at weaning age (P21).

(C) Immunohistochemical staining for NK1R (first column) and SST (second column) on coronal sections from $Jmjd3^{-/-}$ (upper row) and $Jmjd3^{-/-}$;$Rosa26^{Jmjd3}$ (lower row) E18.5 brainstems. A merged image of NK1R (magenta) and SST (green) is shown in the last column on the right. Scale bars represent 100 μm.

See also Figure S4.

loss of JMJD3, suggesting that loss of JMJD3 may impair PBC maturation also through defective formation of the 5-HT system (Figure 4H). However, since the development and function of the RTN/pFRG was not affected by JMJD3 loss, we must conclude that PBC failure results mainly from the selective requirement of JMJD3 for its maintenance.

Exogenous Expression of JMJD3 Rescues the Perinatal Lethality Caused by the *Jmjd3* Knockout Allele

In order to gain unequivocal evidence that the respiratory failure and the lack of PBC maintenance in our mutants were caused by lack of JMJD3, we sought to rescue the phenotype by re-expressing *Jmjd3*. To this end, we engineered a mouse strain for the Cre-loxP-dependent expression of *Jmjd3* from the *Rosa26* (R26) genomic locus (Figure 5A). Following identification of homologous recombinant ESC clones (Figure S4), we derived chimeras that transmitted the allele through the germline (hereafter $Rosa26^{flSTOP\text{-}Jmjd3}$). We then bred the $Rosa26^{flSTOP\text{-}Jmjd3}$ allele into the *Jmjd3* knockout strain along with a ubiquitous Cre-deleter strain to check whether the recombined *Jmjd3* transgene ($Rosa26^{Jmjd3}$) was able to rescue perinatal lethality. As shown in Figure 5B, mice homozygous for the gene trap allele

(six PBC/genotype). Shown is, for the value of each level, the mean ± SD; asterisks indicate statistically significant differences (*$p < 0.05$, **$p < 0.01$, Student's t test).

(E) Overlay of immunohistochemical staining for NK1R (red) and *Jmjd3* (RNA in situ hybridization, blue). NK1R staining and *Jmjd3 in situ* hybridization were performed on consecutive sagittal sections from wild-type E18.5 brainstem and the images from the same area were aligned with respect to the ventral limit of the medulla.

(F) Histogram showing the percentage of $Jmjd3^{+/+}$, $Jmjd3^{+/-}$ and $Jmjd3^{-/-}$ preparations with attached rib cage that did (white bars) or did not (black bars) produce rhythmic diaphragmatic EMG bursts at E15.5, E16.5 and E18.5. The number of preparations analyzed is indicated in each bar. The percentage of active preparations with rhythmic EMG bursts decreased with maturational age in $Jmjd3^{-/-}$ embryos, whereas it remained constant in $Jmjd3^{+/+}$ and $Jmjd3^{+/-}$ embryos.

(G) Immunohistochemical staining for NK1R (first column) and SST (second column) on coronal sections from $Jmjd3^{+/+}$ and $Jmjd3^{-/-}$ E16.5 brainstems.

(H) Histogram showing the brainstem content of the 5-HT precursor L-Trp, 5-HT and the metabolite 5-HIAA in $Jmjd3^{+/+}$ ($n = 8$), $Jmjd3^{+/-}$ ($n = 10$) and $Jmjd3^{-/-}$ ($n = 8$) embryos at E16.5. Brainstem levels of 5-HT and 5-HIAA were significantly lower in $Jmjd3^{-/-}$ embryos than in $Jmjd3^{+/+}$ and $Jmjd3^{+/-}$ embryos, whereas L-Trp content was similar for all three genotypes. Bars represent the mean ± SEM and asterisks indicate statistically significant differences ($p < 0.05$, Student's t test). Scale bars represent 100 μm (A, C, G) and 10 μm (E). *nA*: nucleus ambiguus, *PBC*: pre-Bötzinger complex, *VII*: facial motor nucleus.

See also Figure S3.

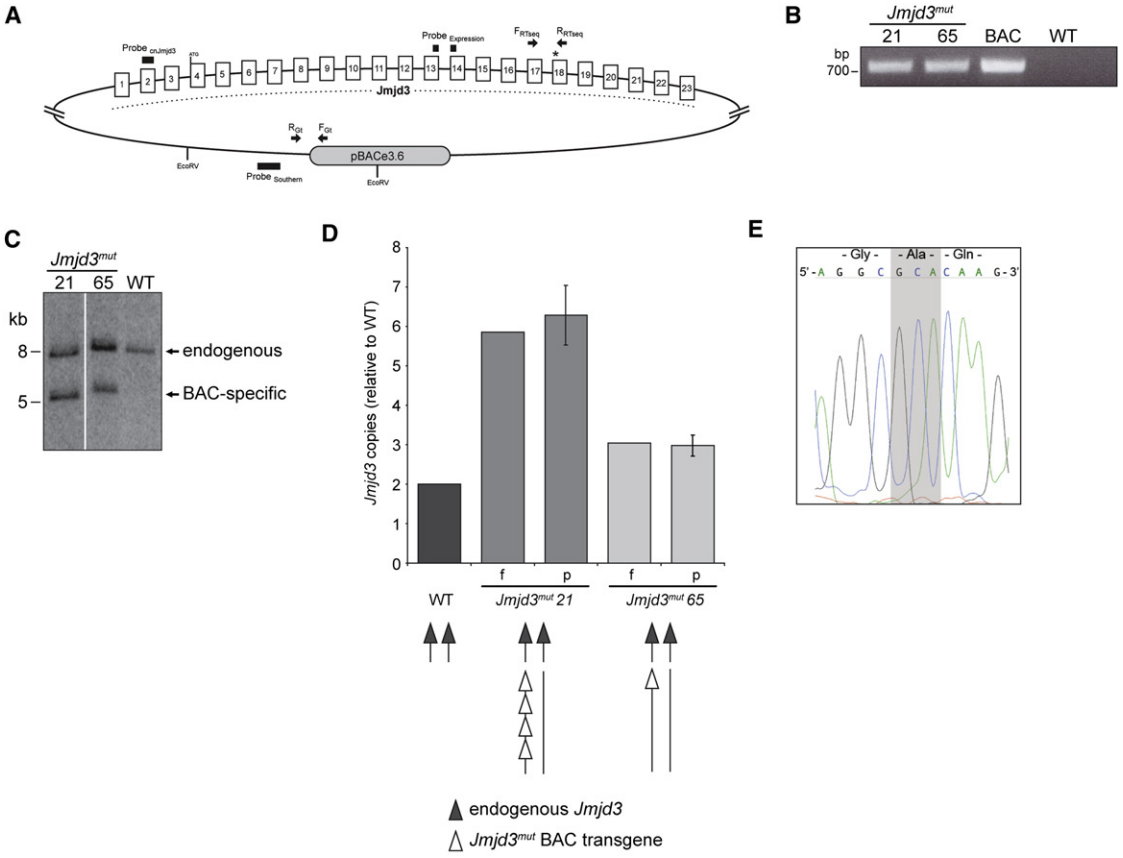

F

		Jmjd3	+/+		+/-		-/-	
		Jmjd3mut	+	-	+	-	+	-
Jmjd3+/-;Jmjd3mut × Jmjd3+/-;Jmjd3mut	Jmjd3mut 21	observed (n=44) [a]	19	2	16	7	0	0
		[%]	(43.2)	(4.5)	(36.4)	(15.9)	(0)	(0)
	Jmjd3mut 65	observed (n=39) [a]	6	2	20	11	0	0
		[%]	(15.4)	(5.1)	(51.3)	(28.2)	(0)	(0)
		expected [%]	18.75	6.25	37.5	12.5	18.75	6.25

[a] highly significantly different from expected distribution of genotypes (Chi-square test, $p < 0.01$)

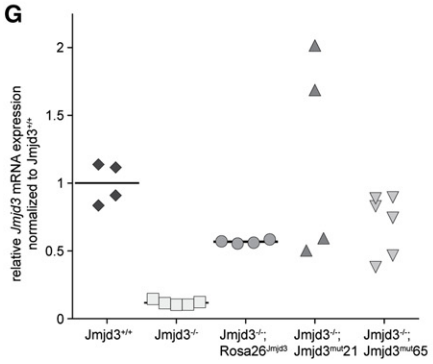

Figure 6. The Enzymatic Activity of JMJD3 Is Required for the Maintenance of the Respiratory Network

(A) Schematic representation of the BAC harboring the *Jmjd3* locus engineered with a point mutation. Shown are the pBACe3.6 vector (gray oval), *Jmjd3* exons (white numbered rectangles), oligos used for genotyping (F_{Gt} and R_{Gt}), oligos used to amplify cDNA for sequencing of the point mutation (F_{RTseq} and R_{RTseq}), probe used for Southern blot ($Probe_{Southern}$), TaqMan copy number probe ($Probe_{cnJmjd3}$), and TaqMan gene expression probe ($Probe_{Expression}$).

(B) PCR-based screening of *Jmjd3*^{mut} transgenic mice, showing the amplification of a *Jmjd3*^{mut} BAC-specific 710 bp PCR product in two independent founder lines (*Jmjd3*^{mut}21 and *Jmjd3*^{mut}65).

(*Jmjd3*$^{-/-}$) and harboring the *Rosa26*^{Jmjd3} allele reached weaning age at the correct Mendelian ratios. While this provided conclusive evidence that the expression of JMJD3 suffices to rescue RRG function, we confirmed this rescue also with the immunohistochemical characterization of a normal PBC in *Jmjd3*$^{-/-}$;*Rosa26*^{Jmjd3} compound mutants at E18.5 (Figure 5C).

Maintenance of the Respiratory Network Requires the Enzymatic Activity of JMJD3

The relative inefficiency of demethylation catalyzed by JmjC domain-containing enzymes, along with their often limited contribution to the global levels of histone methylation and gene transcription, led us to hypothesize that JmjC domain-containing demethylases may function also independent of enzymatic activity (Natoli et al., 2009). Genome-wide analysis in macrophages confirmed that JMJD3 could regulate gene expression also in a demethylation-independent manner (De Santa et al., 2009), as subsequently established also for its demethylase-independent role in chromatin remodeling (Miller et al., 2010) and more recently for its regulation of gene expression in promyelocytic leukemia (Chen et al., 2012). We thus aimed at determining whether the catalytic function of JMJD3 was required for the maintenance of the PBC. To this end, we isolated a bacterial artificial chromosome (BAC) harboring the *Jmjd3* locus (Figure 6A) and engineered through ''recombineering'' a point mutation resulting in a Histidine to Alanine substitution at codon 1388, which abolishes catalysis by the JmjC domain. We screened oocyte injection-derived transgenic mutant-*Jmjd3* mice (hereafter *Jmjd3*^{mut}) by PCR (Figure 6B) and estimated the number of integrations by Southern blot (Figure 6C), using a probe that enabled comparison of the signal from the endogenous sequence with that from the BAC-specific one (Figure 6A). As the Southern probe was not located in close proximity of the *Jmjd3* gene, we confirmed the copy number range with a quantitative PCR (qPCR) probe spanning the second exon of *Jmjd3* and hence providing a direct estimate of the number of extra *Jmjd3* integrated copies. As shown in Figure 6D, qPCR confirmed that *Jmjd3*^{mut}21 and *Jmjd3*^{mut}65 had, respectively, four and one extra copies of the *Jmjd3* locus that were transmitted stably across generations (Figure 6D).

Next, we confirmed the expression of the mutant *Jmjd3* allele by sequencing a RT-PCR product spanning the mutated codon and amplified from the brain of *Jmjd3*^{mut}21 and *Jmjd3*^{mut}65 mice (Figure 6E). Finally, we intercrossed mice heterozygous for the *Jmjd3* knockout allele (*Jmjd3*$^{+/-}$) and harboring either *Jmjd3*^{mut}21 or *Jmjd3*^{mut}65. As shown in Figure 6F, despite the expected segregation of either *Jmjd3*^{mut} allele among both *Jmjd3*$^{+/+}$ and *Jmjd3*$^{+/-}$ animals, we were unable to retrieve at weaning age any compound *Jmjd3*$^{-/-}$;*Jmjd3*^{mut}21 or *Jmjd3*$^{-/-}$;*Jmjd3*^{mut}65 mutants, whereas we could readily obtain them at embryonic day E18.5 (Figure S5). Importantly, in the brains of both these E18.5 *Jmjd3*$^{-/-}$;*Jmjd3*^{mut}21 and *Jmjd3*$^{-/-}$;*Jmjd3*^{mut}65 compound mutants, we confirmed that the BAC transgenes rescued the expression of *Jmjd3* at least to the level observed in *Jmjd3*$^{-/-}$;*Rosa26*^{Jmjd3} embryos (Figure 6G). This allows us to conclude that the expression of catalytically inactive JMJD3 cannot compensate for the loss of the wild-type protein.

JMJD3 Regulates Critical PBC-Specific Genes through H3K27me3 Demethylation

To gain mechanistic insight into the downstream targets through which the enzymatic activity of JMJD3 controls PBC maintenance and function, we started from the recent identification, by cDNA subtraction, of thus far the most extensive subset of rodent PBC-specific markers. Besides identifying several PBC markers in addition to NK1R and SST, this study characterized the glycoprotein Reelin for its high and selective expression in a subset of PBC NK1R- and SST-positive neurons and for its requirement in PBC-mediated response to hypoxia (Solomon et al., 2000; Tan et al., 2012). We thus carried out a meta-analysis of available data sets to interrogate the dynamics of H3K27me3 at the promoter of these PBC-specific genes during neural differentiation, reasoning that this would guide us in predicting which PBC-relevant genes are most likely impacted by failed H3K27me3 demethylation. Importantly, this meta-analysis included expression and genome-wide chromatin profiles from the homogeneous differentiation of ESC into terminally differentiated glutamatergic neurons (N) through intermediate cell aggregate (CA) and neural precursor (NP) stages, a relevant experimental system given the glutamatergic nature of PBC neurons and the one that first exposed H3K27me3 dynamics during neuronal differentiation (Bibel et al., 2004; Mohn et al., 2008). We retrieved several PBC-specific genes that lost H3K27me3 in the transition from ESC to N, including Reelin (*Reln*), membrane-associated Ring Finger 4 *(March4),* kin of IRRE-like 3 *(Kirrel3,* also known as *Neph2*), and estrogen-related receptor gamma *(Esrrg)* and set out to validate the role of JMJD3 in their regulation starting from wild-type and *Jmjd3*$^{-/-}$ ESC. As shown in Figure 7A, all four genes were virtually silent in wild-type ESC, peaked in NP and returned to intermediate levels in N,

(C) Southern blot of EcoRV-digested genomic DNA from *Jmjd3*^{mut}21, *Jmjd3*^{mut}65 and C57BL/6 (WT control) mouse tails. The endogenous *Jmjd3* locus and the *Jmjd3*^{mut} BAC yielded fragments of, respectively, 7.7 and 5.1 kb.

(D) Quantitation of the number of BAC copies integrated in the *Jmjd3*^{mut}21 and *Jmjd3*^{mut}65 founders (f) and their progenies (p) assessed by real-time PCR using Probe$_{cnJmjd3}$. The scheme illustrates the number of BAC-harbored *Jmjd3* copies present in the wild-type control (two endogenous copies), *Jmjd3*^{mut}21 strain (six copies in total) and *Jmjd3*^{mut}65 strain (three copies in total). Bars for (p) represent the mean ± SD of n = 5 mice.

(E) Sequencing trace of the RT-PCR product amplified from the brain, spanning exons 17 and 18 and demonstrating expression of the point mutation (highlighted in gray) resulting in the Histidine to Alanine substitution at position 1388.

(F) Table showing the lack of phenotypic rescue by catalytically inert JMJD3, assessed by genotyping mice recovered at weaning age and derived from heterozygous crossings between *Jmjd3*$^{+/-}$ mice carrying either the *Jmjd3*^{mut}21 or the *Jmjd3*^{mut}65 transgene. Statistical analysis was performed with Chi-square test.

(G) qRT-PCR analysis of *Jmjd3* mRNA expression in brains from E18.5 *Jmjd3*$^{+/+}$, *Jmjd3*$^{-/-}$, *Jmjd3*$^{-/-}$;*Rosa26*^{Jmjd3}, *Jmjd3*$^{-/-}$;*Jmjd3*^{mut}21, and *Jmjd3*$^{-/-}$;*Jmjd3*^{mut}65 embryos.

See also Figure S5.

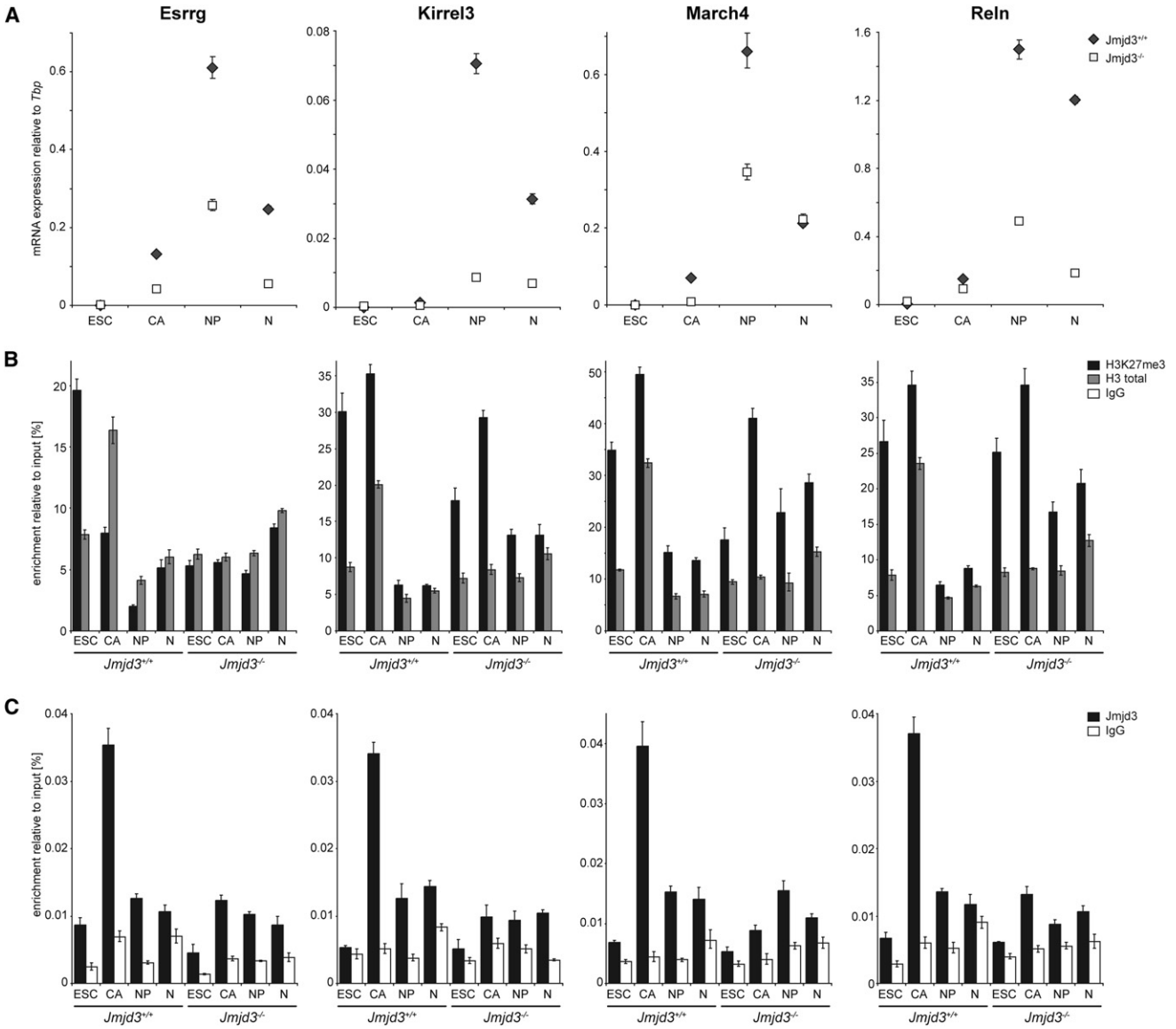

Figure 7. JMJD3 Regulates PBC-Relevant Genes during the Acquisition of Glutamatergic Neuronal Fate

(A) Expression profiles of *Esrrg*, *Kirrel3*, *March4*, and *Reln* during differentiation of wild-type and *Jmjd3*$^{-/-}$ ESC into glutamatergic neurons through cell aggregate and neural precursor intermediates. Shown are the means ± SD of qRT-PCR triplicates normalized to *Tbp*.

(B) Enrichment for H3K27me3 at the promoters of *Esrrg*, *Kirrel3*, *March4*, and *Reln* in ESC, CA, NP, and N along with H3 occupancy. Bars represent the means ± SD of qPCR triplicates in a representative ChIP experiment.

(C) Assessment of JMJD3 binding to the promoters of *Esrrg*, *Kirrel3*, *March4*, and *Reln* in ESC, CA, NP, and N. *ESC*, embryonic stem cells; *CA*, cell aggregates at day 8 of differentiation; *NP*, neural precursors following plating of CA at day 10 of differentiation; *N*, neurons. Bars represent the means ± SD of qPCR triplicates in a representative ChIP experiment.

but their upregulation was virtually completely abolished upon loss of JMJD3. We next examined the dynamics of H3K27me3 in ESC, CA, NP, and N (Figure 7B). While in wild-type cells H3K27me3 (controlled for H3 occupancy) underwent a dramatic decrease in the transition from ESC through CA to NP and N, its levels dropped significantly less (*Kirrel3* and *Reln*) or remained stable (*March4* and *Esrrg*) in *Jmjd3*$^{-/-}$ cells, indicating impaired H3K27me3 demethylation (Figure 7B). Consistently, and in agreement with its expression pattern (data not shown), JMJD3 recruitment peaked at the CA stage and was severely compromised in mutants (Figure 7C).

We can thus conclude that during the in vitro acquisition of glutamatergic fate, a hallmark feature of PBC neurons required for rhythm generation, JMJD3 controls the expression of critical PBC-specific genes through H3K27me3 demethylation, a function that we hypothesize to become eventually rate-limiting for the maintenance of PBC function in vivo. *Reln* and *Kirrel3* are in this respect particularly relevant targets, given the involvement

of the former in PBC-mediated hypoxic response and the role of the latter in structuring the pontine nucleus by controlling the late stages of neuronal migration (Nishida et al., 2011).

DISCUSSION

The dynamics of Polycomb marking during neurogenesis suggested a critical role for timed H3K27 demethylation in the acquisition of neural fate (Mohn et al., 2008; Testa, 2011). Direct regulation by the H3K27 demethylase JMJD3 of key neurogenic factors during mouse ESC neurulation and chick spinal cord development confirmed the role of this enzyme in early neural development (Akizu et al., 2010; Burgold et al., 2008); yet its in vivo function in the emergence and maturation of the mammalian CNS remained unexplored. Through genetic inactivation of *Jmjd3* in the mouse, our work uncovers an unanticipated role of this enzyme in the maintenance of the embryonic respiratory neuronal network, extending the relevance of its enzymatic activity from early lineage choices to the late structuring of neuronal networks.

We found that truncation of the *Jmjd3* transcript downstream of its first noncoding exon results in perinatal lethality with full penetrance. This finding, apparently at odds with JMJD3 requirement for early developmental choices (Canovas et al., 2012), suggests that the partial efficiency of the trap cassette in ESC guarantees levels of the protein that apparently suffice to carry through the earliest stages of development. Interestingly, selective ablation of the JmjC domain also resulted in perinatal lethality, indicating that at least the enzymatic portion of JMJD3 may be surprisingly dispensable for early mouse development (Satoh et al., 2010).

Our findings establish that JMJD3 is selectively required for the maintenance and function of the PBC component of the RRG and uncover critical PBC-specific genes that are targets of JMJD3 during the acquisition of glutamatergic neuronal fate. Electrophysiological and immunohistochemical studies of *Jmjd3*-null embryos at E15.5, E16.5, and E18.5 revealed that the early stages of RRG development took place normally despite the lack of JMJD3. In *Jmjd3*-null embryos at E15.5, the RRG was able to produce a rhythmic respiratory drive and to adapt it to pH changes, revealing a normal function of the RTN/pFRG and PBC oscillators just after their emergence. From E15.5 onward, however, lack of JMJD3 impaired progressively the further maturation and rhythmogenicity of the PBC, which became silent in half of *Jmjd3*-null embryos at E16.5 and in all *Jmjd3*-null embryos at E18.5. This functional decay upon loss of JMJD3 was mirrored in the network structure of the PBC, which was still comparatively well preserved at E16.5 but appeared severely disrupted at E18.5, with dramatic defects in the number and architecture of NK1R- and SST-positive neurons. Finally, we identified several PBC-specific genes that depend on JMJD3 for H3K27 demethylation-dependent upregulation during neuronal differentiation. Importantly, these include Reelin, coding for the glycoprotein involved in PBC response to hypoxia, and Kirrel3, a member of the immunoglobulin superfamily involved in the late phases of neuronal migration underlying the architecture of hindbrain nuclei. Thus, in light of the paucity of functionally validated PBC markers, our approach also establishes the differentiation of ESC into glutamatergic neurons as a paradigm to uncover and validate PBC-relevant genes.

Several features of this phenotype appear particularly striking in relation to previously reported gene-specific respiratory deficits. The first is the selectivity in PBC impairment. Thus, mutations in the transcription factor DBX1 and the axon guidance receptor ROBO3 produced no rhythmic phrenic bursts because of alterations of brainstem crossed pathways impairing the production of the respiratory central drive toward phrenic motoneurons (Bouvier et al., 2010). Crossed pathways were instead spared in *Jmjd3* mutants, just like the RTN/pFRG nucleus.

Second, the severity of the phenotype, with the complete lack of RRG activity at E18.5, also stands in contrast with the phenotypes observed in most other respiratory mutants, including *Mash1*, *Phox2a*, *Phox2b*, *Rnx*, *Hoxa1*, *Krox20*, *Ret*, and *MafB*, which presented in varying degrees severe aberrations but not a complete absence of respiratory activity. This difference appears particularly relevant in the case of the transcription factor MAFB, whose phenotypic features (perinatal gasping behavior coupled to an abnormally structured PBC) led to posit the emergence in late gestation of rhythmogenic MAFB-dependent neurons (Blanchi et al., 2003). However, despite the fact that also JMJD3 is required for the late structuring of the PBC, we can exclude a downstream involvement of MAFB in our mutants since in *MafB*-null E18.5 embryos the RRG was active and produced a gasping-like rhythm (Blanchi et al., 2003). The observation that this along with most other respiratory mutants maintained the generation of inspiratory bursts, albeit at much reduced frequency, led to the suggestion that the mechanisms underlying the production of such bursts may be particularly resilient even in the context of aberrantly developed respiratory circuits (Blanchi et al., 2003; Wallén-Mackenzie et al., 2006). Indeed, the only mutant with a complete ablation of synchronized PBC activity had been thus far that resulting from the inactivation of vesicular glutamate transporter 2 (*VGlut2*) (Wallén-Mackenzie et al., 2006). Critically, however, in this mutant the PBC never began functioning although it appeared morphologically normal. Hence loss of JMJD3 represents the first instance of a complete ablation of PBC activity which intervenes however after its normal emergence at day E15.5.

This last feature involves the role of JMJD3 in the maintenance or late maturation of the PBC and appears particularly relevant in the light of genetic evidence that defined for the Trithorax family of proteins a selective role in the maintenance rather than in the establishment of gene expression patterns and body segment identities (Glaser et al., 2006; Kennison, 1995; Yu et al., 1998). Given our previous characterization of the association between JMJD3 and the core components of the Trithorax MLL1/4 complexes (De Santa et al., 2007), the late requirement for JMJD3 in PBC structure and function extends now the Trithorax paradigm from the maintenance of gene expression patterns in early development to the stability of neuronal networks in late gestation.

Finally, previous studies, including our own, had suggested that JMJD3 could also function independent of its enzymatic activity (Burgold et al., 2008; De Santa et al., 2009; Miller et al., 2010; Natoli et al., 2009). Thus, it became critical to test whether the role of JMJD3 in PBC maintenance requires its enzymatic

activity. Our results provide conclusive evidence that it does, uncovering a vital function for the catalytic properties of this protein.

EXPERIMENTAL PROCEDURES

Murine Strains

Experiments involving animals were performed in accordance with the Italian and French Laws that enforce EU 86/609 Directive (Council Directive 86/609/EEC of 24 November 1986 on the approximation of laws, regulations and administrative provisions of the Member States regarding the protection of animals used for experimental and other scientific purposes). All strains used in this study were bred into C57BL/6 background. The day of vaginal plug was considered to be E0.5. Analysis of the phenotype and genotype were performed independently in blind experiments and compared afterward.

The mouse ESC line XB814 harboring a gene trap insertion in *Jmjd3* was obtained from BayGenomics (http://www.mmrrc.org/catalog/overview_BG.php) (Stryke et al., 2003) and the insertion site of the trap cassette was mapped to *Jmjd3* intron 1 by sequence analysis. ESCs were injected into C57BL/6 blastocysts to generate chimeras following standard procedures (Nagy et al., 2003). Germline transmission was confirmed by PCR on genomic DNA extracted from tail biopsies using the primers Forw1, Rev1, and Rev2 (Table S1). The *Rosa26*$^{flSTOP\text{-}Jmjd3}$ and BAC transgenic *Jmjd3*^{mut} strains are described in Extended Experimental Procedures.

Immunohistochemistry and 3D Reconstruction

Detailed immunohistochemistry procedures are described in the Extended Experimental Procedures. For 3D reconstructions we used the software Reconstruct (Fiala, 2005). Consecutive coronal sections (each 8 μm thick) from brainstems of E18.5 *Jmjd3*$^{+/+}$ and *Jmjd3*$^{-/-}$ embryos were stained for NK1R and SST. Images were aligned manually and NK1R-positive cells were defined using the Wildfire tool with the same threshold settings for all images. 3D visualization was generated by stacking the traces defined in each section.

Respiratory In Vivo and In Vitro Studies

As previously reported (Blanchi et al., 2003; Caubit et al., 2010; Ren et al., 2003), in vivo and in vitro approaches were used to examine the respiratory system of mouse embryos after surgical delivery at gestational days E15.5, E16.5, and E18.5. At E18.5, whole-body plethysmography (EMKA technologies, Paris, France) was used to record in vivo breathing movements for 3–5 min, just after delivery. Plethysmographic chambers were maintained at 32°C and embryonic mouth temperature monitored with miniature thermistor nylon-coated probe. Thin cooper wires inserted within intercostal muscles allowed recordings of chest EMG and ECG in either E18.5 embryos kept in utero with preserved umbilical irrigation or younger embryos studied in vitro. For in vitro experiments, the medulla and cervical cord of E18.5 embryos were dissected, placed in a 2 ml chamber, superfused with carbogenated aCSF (4 ml/min, 26°C [pH 7.4]) and the C4 root of the phrenic nerve was sucked within a glass micropipette to record rhythmic PBs. In younger embryos where the C4 root was especially fragile, the rib cage was retained in vitro to allow visualization of chest contractions and recording of chest respiratory EMG. Control aCSF was occasionally replaced by acidified aCSF (pH 7.1), aCSF containing drugs or aCSF with elevated concentration of potassium for 5–10 min. Electrical stimulations were applied via tungsten microelectrodes to the diaphragm or phrenic nerve to check the embryonic neuromuscular system and to the spinal cord or medulla to check the neural excitability and synaptic transmission of the embryonic medullospinal pathways. In addition, brainstems of E16.5 embryos were dissected and used for HPLC biochemical analysis of serotonin metabolism (Menuet et al., 2011).

SUPPLEMENTAL INFORMATION

Supplemental Information includes Extended Experimental Procedures, five figures, one table, and one movie and can be found with this article online at http://dx.doi.org/10.1016/j.celrep.2012.09.013.

LICENSING INFORMATION

ACKNOWLEDGMENTS

We thank Alastair D. Morrison and Philip D. Hayes (GlaxoSmithKline Research and Development), and Sigrun Murr and Elisa Allievi (IFOM-IEO Campus Transgenic facility) for technical help and support. This work was supported by grants from the Italian Association for Cancer Research (AIRC) (G.T., S.C., and G.N.), the Italian Health Ministry (G.T. and S.C.), the Italian Foundation for Cancer Research (FIRC) (P.P.T., G.T., and S.C.), the Association for International Cancer Research (AICR) (G.T.), the Italian Ministry for Education, University and Research (S.C.) and the Centre National de la Recherche Scientifique (UMR 6231, G.H.). G.T. conceived the study; T.B. generated the Jmjd3 knockout strain and performed the experiments along with N.V., C.M., M.B., C.G., and G.H. who performed the electrophysiological characterization; M.C. and S.C. generated the *Rosa26*$^{flSTOP\text{-}Jmjd3}$ strain; P.P.T. generated and characterized the *Jmjd3*^{mut} BAC transgenic strains; B.K.T., F.S., S.B., G.N., and L.K. provided reagents and helped with the characterization of cells and mice; A.S. performed in situ hybridizations; T.B., N.V., G.H., and G.T. analyzed the data; G.T. wrote the paper.

Received: February 5, 2012
Revised: July 10, 2012
Accepted: September 12, 2012
Published: October 25, 2012

REFERENCES

Agger, K., Cloos, P.A., Christensen, J., Pasini, D., Rose, S., Rappsilber, J., Issaeva, I., Canaani, E., Salcini, A.E., and Helin, K. (2007). UTX and JMJD3 are histone H3K27 demethylases involved in HOX gene regulation and development. Nature *449*, 731–734.

Akizu, N., Estarás, C., Guerrero, L., Martí, E., and Martínez-Balbás, M.A. (2010). H3K27me3 regulates BMP activity in developing spinal cord. Development *137*, 2915–2925.

Amiel, J., Dubreuil, V., Ramanantsoa, N., Fortin, G., Gallego, J., Brunet, J.F., and Goridis, C. (2009). PHOX2B in respiratory control: lessons from congenital central hypoventilation syndrome and its mouse models. Respir. Physiol. Neurobiol. *168*, 125–132.

Bibel, M., Richter, J., Schrenk, K., Tucker, K.L., Staiger, V., Korte, M., Goetz, M., and Barde, Y.A. (2004). Differentiation of mouse embryonic stem cells into a defined neuronal lineage. Nat. Neurosci. *7*, 1003–1009.

Blanchi, B., Kelly, L.M., Viemari, J.C., Lafon, I., Burnet, H., Bévengut, M., Tillmanns, S., Daniel, L., Graf, T., Hilaire, G., and Sieweke, M.H. (2003). MafB deficiency causes defective respiratory rhythmogenesis and fatal central apnea at birth. Nat. Neurosci. *6*, 1091–1100.

Bou-Flores, C., Lajard, A.M., Monteau, R., De Maeyer, E., Seif, I., Lanoir, J., and Hilaire, G. (2000). Abnormal phrenic motoneuron activity and morphology in neonatal monoamine oxidase A-deficient transgenic mice: possible role of a serotonin excess. J. Neurosci. *20*, 4646–4656.

Bouvier, J., Thoby-Brisson, M., Renier, N., Dubreuil, V., Ericson, J., Champagnat, J., Pierani, A., Chédotal, A., and Fortin, G. (2010). Hindbrain interneurons and axon guidance signaling critical for breathing. Nat. Neurosci. *13*, 1066–1074.

Burgold, T., Spreafico, F., De Santa, F., Totaro, M.G., Prosperini, E., Natoli, G., and Testa, G. (2008). The histone H3 lysine 27-specific demethylase Jmjd3 is required for neural commitment. PLoS ONE *3*, e3034.

Byvoet, P., Shepherd, G.R., Hardin, J.M., and Noland, B.J. (1972). The distribution and turnover of labeled methyl groups in histone fractions of cultured mammalian cells. Arch. Biochem. Biophys. *148*, 558–567.

Canovas, S., Cibelli, J.B., and Ross, P.J. (2012). Jumonji domain-containing protein 3 regulates histone 3 lysine 27 methylation during bovine preimplantation development. Proc. Natl. Acad. Sci. USA *109*, 2400–2405.

Caubit, X., Thoby-Brisson, M., Voituron, N., Filippi, P., Bévengut, M., Faralli, H., Zanella, S., Fortin, G., Hilaire, G., and Fasano, L. (2010). Teashirt 3 regulates development of neurons involved in both respiratory rhythm and airflow control. J. Neurosci. *30*, 9465–9476.

Chen, S., Ma, J., Wu, F., Xiong, L.J., Ma, H., Xu, W., Lv, R., Li, X., Villen, J., Gygi, S.P., et al. (2012). The histone H3 Lys 27 demethylase JMJD3 regulates gene expression by impacting transcriptional elongation. Genes Dev. *26*, 1364–1375.

De Santa, F., Totaro, M.G., Prosperini, E., Notarbartolo, S., Testa, G., and Natoli, G. (2007). The histone H3 lysine-27 demethylase Jmjd3 links inflammation to inhibition of polycomb-mediated gene silencing. Cell *130*, 1083–1094.

De Santa, F., Narang, V., Yap, Z.H., Tusi, B.K., Burgold, T., Austenaa, L., Bucci, G., Caganova, M., Notarbartolo, S., Casola, S., et al. (2009). Jmjd3 contributes to the control of gene expression in LPS-activated macrophages. EMBO J. *28*, 3341–3352.

Fiala, J.C. (2005). Reconstruct: a free editor for serial section microscopy. J. Microsc. *218*, 52–61.

Fortin, G., and Thoby-Brisson, M. (2009). Embryonic emergence of the respiratory rhythm generator. Respir. Physiol. Neurobiol. *168*, 86–91.

Gaspar, P., Cases, O., and Maroteaux, L. (2003). The developmental role of serotonin: news from mouse molecular genetics. Nat. Rev. Neurosci. *4*, 1002–1012.

Gestreau, C., Heitzmann, D., Thomas, J., Dubreuil, V., Bandulik, S., Reichold, M., Bendahhou, S., Pierson, P., Sterner, C., Peyronnet-Roux, J., et al. (2010). Task2 potassium channels set central respiratory CO2 and O2 sensitivity. Proc. Natl. Acad. Sci. USA *107*, 2325–2330.

Glaser, S., Schaft, J., Lubitz, S., Vintersten, K., van der Hoeven, F., Tufteland, K.R., Aasland, R., Anastassiadis, K., Ang, S.L., and Stewart, A.F. (2006). Multiple epigenetic maintenance factors implicated by the loss of Mll2 in mouse development. Development *133*, 1423–1432.

Gray, P.A., Janczewski, W.A., Mellen, N., McCrimmon, D.R., and Feldman, J.L. (2001). Normal breathing requires preBötzinger complex neurokinin-1 receptor-expressing neurons. Nat. Neurosci. *4*, 927–930.

Gray, P.A., Fu, H., Luo, P., Zhao, Q., Yu, J., Ferrari, A., Tenzen, T., Yuk, D.I., Tsung, E.F., Cai, Z., et al. (2004). Mouse brain organization revealed through direct genome-scale TF expression analysis. Science *306*, 2255–2257.

Gray, P.A., Hayes, J.A., Ling, G.Y., Llona, I., Tupal, S., Picardo, M.C., Ross, S.E., Hirata, T., Corbin, J.G., Eugenín, J., and Del Negro, C.A. (2010). Developmental origin of preBötzinger complex respiratory neurons. J. Neurosci. *30*, 14883–14895.

Hansen, K.H., Bracken, A.P., Pasini, D., Dietrich, N., Gehani, S.S., Monrad, A., Rappsilber, J., Lerdrup, M., and Helin, K. (2008). A model for transmission of the H3K27me3 epigenetic mark. Nat. Cell Biol. *10*, 1291–1300.

Hilaire, G., Voituron, N., Menuet, C., Ichiyama, R.M., Subramanian, H.H., and Dutschmann, M. (2010). The role of serotonin in respiratory function and dysfunction. Respir. Physiol. Neurobiol. *174*, 76–88.

Hirabayashi, Y., Suzki, N., Tsuboi, M., Endo, T.A., Toyoda, T., Shinga, J., Koseki, H., Vidal, M., and Gotoh, Y. (2009). Polycomb limits the neurogenic competence of neural precursor cells to promote astrogenic fate transition. Neuron *63*, 600–613.

Hunt, P.N., McCabe, A.K., and Bosma, M.M. (2005). Midline serotonergic neurones contribute to widespread synchronized activity in embryonic mouse hindbrain. J. Physiol. *566*, 807–819.

Jepsen, K., Solum, D., Zhou, T., McEvilly, R.J., Kim, H.J., Glass, C.K., Hermanson, O., and Rosenfeld, M.G. (2007). SMRT-mediated repression of an H3K27 demethylase in progression from neural stem cell to neuron. Nature *450*, 415–419.

Kennison, J.A. (1995). The Polycomb and trithorax group proteins of Drosophila: trans-regulators of homeotic gene function. Annu. Rev. Genet. *29*, 289–303.

Lan, F., Bayliss, P.E., Rinn, J.L., Whetstine, J.R., Wang, J.K., Chen, S., Iwase, S., Alpatov, R., Issaeva, I., Canaani, E., et al. (2007). A histone H3 lysine 27 demethylase regulates animal posterior development. Nature *449*, 689–694.

Margueron, R., Justin, N., Ohno, K., Sharpe, M.L., Son, J., Drury, W.J., 3rd, Voigt, P., Martin, S.R., Taylor, W.R., De Marco, V., et al. (2009). Role of the polycomb protein EED in the propagation of repressive histone marks. Nature *461*, 762–767.

Menuet, C., Borghgraef, P., Matarazzo, V., Gielis, L., Lajard, A.M., Voituron, N., Gestreau, C., Dutschmann, M., Van Leuven, F., and Hilaire, G. (2011). Raphé tauopathy alters serotonin metabolism and breathing activity in terminal Tau.P301L mice: possible implications for tauopathies and Alzheimer's disease. Respir. Physiol. Neurobiol. *178*, 290–303.

Miller, S.A., Mohn, S.E., and Weinmann, A.S. (2010). Jmjd3 and UTX play a demethylase-independent role in chromatin remodeling to regulate T-box family member-dependent gene expression. Mol. Cell *40*, 594–605.

Mohn, F., Weber, M., Rebhan, M., Roloff, T.C., Richter, J., Stadler, M.B., Bibel, M., and Schübeler, D. (2008). Lineage-specific polycomb targets and de novo DNA methylation define restriction and potential of neuronal progenitors. Mol. Cell *30*, 755–766.

Nagy, A., Gertsenstein, M., Vintersten, K., and Behringer, R. (2003). Manipulating the Mouse Embryo: A Laboratory Manual, Third Edition (Cold Spring Harbor, NY: Cold Spring Harbor Laboratory Press).

Natoli, G., Testa, G., and De Santa, F. (2009). The future therapeutic potential of histone demethylases: A critical analysis. Curr. Opin. Drug Discov. Devel. *12*, 607–615.

Nishida, K., Nakayama, K., Yoshimura, S., and Murakami, F. (2011). Role of Neph2 in pontine nuclei formation in the developing hindbrain. Mol. Cell. Neurosci. *46*, 662–670.

Onimaru, H., Ikeda, K., and Kawakami, K. (2009). Phox2b, RTN/pFRG neurons and respiratory rhythmogenesis. Respir. Physiol. Neurobiol. *168*, 13–18.

Pereira, J.D., Sansom, S.N., Smith, J., Dobenecker, M.W., Tarakhovsky, A., and Livesey, F.J. (2010). Ezh2, the histone methyltransferase of PRC2, regulates the balance between self-renewal and differentiation in the cerebral cortex. Proc. Natl. Acad. Sci. USA *107*, 15957–15962.

Ren, J., Lee, S., Pagliardini, S., Gérard, M., Stewart, C.L., Greer, J.J., and Wevrick, R. (2003). Absence of Ndn, encoding the Prader-Willi syndrome-deleted gene necdin, results in congenital deficiency of central respiratory drive in neonatal mice. J. Neurosci. *23*, 1569–1573.

Rose, M.F., Ren, J., Ahmad, K.A., Chao, H.T., Klisch, T.J., Flora, A., Greer, J.J., and Zoghbi, H.Y. (2009). Math1 is essential for the development of hindbrain neurons critical for perinatal breathing. Neuron *64*, 341–354.

Satoh, T., Takeuchi, O., Vandenbon, A., Yasuda, K., Tanaka, Y., Kumagai, Y., Miyake, T., Matsushita, K., Okazaki, T., Saitoh, T., et al. (2010). The Jmjd3-Irf4 axis regulates M2 macrophage polarization and host responses against helminth infection. Nat. Immunol. *11*, 936–944.

Smith, J.C., Ellenberger, H.H., Ballanyi, K., Richter, D.W., and Feldman, J.L. (1991). Pre-Bötzinger complex: a brainstem region that may generate respiratory rhythm in mammals. Science *254*, 726–729.

Solomon, I.C., Edelman, N.H., and Neubauer, J.A. (2000). Pre-Bötzinger complex functions as a central hypoxia chemosensor for respiration in vivo. J. Neurophysiol. *83*, 2854–2868.

Stornetta, R.L., Rosin, D.L., Wang, H., Sevigny, C.P., Weston, M.C., and Guyenet, P.G. (2003). A group of glutamatergic interneurons expressing high levels of both neurokinin-1 receptors and somatostatin identifies the region of the pre-Bötzinger complex. J. Comp. Neurol. *455*, 499–512.

Stryke, D., Kawamoto, M., Huang, C.C., Johns, S.J., King, L.A., Harper, C.A., Meng, E.C., Lee, R.E., Yee, A., L'Italien, L., et al. (2003). BayGenomics: a resource of insertional mutations in mouse embryonic stem cells. Nucleic Acids Res. *31*, 278–281.

Tan, W., Sherman, D., Turesson, J., Shao, X.M., Janczewski, W.A., and Feldman, J.L. (2012). Reelin demarcates a subset of pre-Bötzinger complex neurons in adult rat. J. Comp. Neurol. *520*, 606–619.

Testa, G. (2011). The time of timing: how Polycomb proteins regulate neurogenesis. Bioessays *33*, 519–528.

Thoby-Brisson, M., Karlén, M., Wu, N., Charnay, P., Champagnat, J., and Fortin, G. (2009). Genetic identification of an embryonic parafacial oscillator coupling to the preBötzinger complex. Nat. Neurosci. *12*, 1028–1035.

Thoby-Brisson, M., Trinh, J.B., Champagnat, J., and Fortin, G. (2005). Emergence of the pre-Bötzinger respiratory rhythm generator in the mouse embryo. J. Neurosci. *25*, 4307–4318.

Viemari, J.C., Bévengut, M., Burnet, H., Coulon, P., Pequignot, J.M., Tiveron, M.C., and Hilaire, G. (2004). Phox2a gene, A6 neurons, and noradrenaline are essential for development of normal respiratory rhythm in mice. J. Neurosci. *24*, 928–937.

Wallén-Mackenzie, A., Gezelius, H., Thoby-Brisson, M., Nygård, A., Enjin, A., Fujiyama, F., Fortin, G., and Kullander, K. (2006). Vesicular glutamate transporter 2 is required for central respiratory rhythm generation but not for locomotor central pattern generation. J. Neurosci. *26*, 12294–12307.

Xiang, Y., Zhu, Z., Han, G., Lin, H., Xu, L., and Chen, C.D. (2007). JMJD3 is a histone H3K27 demethylase. Cell Res. *17*, 850–857.

Yu, B.D., Hanson, R.D., Hess, J.L., Horning, S.E., and Korsmeyer, S.J. (1998). MLL, a mammalian trithorax-group gene, functions as a transcriptional maintenance factor in morphogenesis. Proc. Natl. Acad. Sci. USA *95*, 10632–10636.

Zanella, S., Watrin, F., Mebarek, S., Marly, F., Roussel, M., Gire, C., Diene, G., Tauber, M., Muscatelli, F., and Hilaire, G. (2008). Necdin plays a role in the serotonergic modulation of the mouse respiratory network: implication for Prader-Willi syndrome. J. Neurosci. *28*, 1745–1755.